Superconducting nanowire single photon detectors based on NbRe nitride ultrathin films

Avitabile, F.; Colangelo, F.; Mikhailov, M. Yu; Makhdoumi Kakhaki, Z.; Kumar, A.; Esmaeil Zadeh, I.; Attanasio, C.; Cirillo, C.

DOI
10.1063/5.0282478

Publication date
2025

Document Version
Final published version

Published in
Applied Physics Letters

RESEARCH ARTICLE | OCTOBER 28 2025

Superconducting nanowire single photon detectors based on NbRe nitride ultrathin films

F. Avitabile ; F. Colangelo ; M. Yu. Mikhailov ; Z. Makhdoumi Kakhaki ; A. Kumar ; I. Esmaeil Zadeh ; C. Attanasio ; C. Cirillo

Appl. Phys. Lett. 127, 172601 (2025)
https://doi.org/10.1063/5.0282478

Applied Physics Letters ARTICLE pubs.aip.org/aip/apl

Superconducting nanowire single photon detectors based on NbRe nitride ultrathin films

Cite as: Appl. Phys. Lett. **127**, 172601 (2025); doi: 10.1063/5.0282478
Submitted: 26 May 2025 · Accepted: 30 September 2025 ·
Published Online: 28 October 2025

F. Avitabile,[1] F. Colangelo,[1,2,3] M. Yu. Mikhailov,[3] Z. Makhdoumi Kakhaki,[1,2] A. Kumar,[1,2] I. Esmaeil Zadeh,[3] C. Attanasio,[1,2,4] and C. Cirillo[1,a)]

AFFILIATIONS

[1]CNR-SPIN, c/o Università degli Studi di Salerno, I-84084 Fisciano (Sa), Italy
[2]Dipartimento di Fisica "E.R. Caianiello," Università degli Studi di Salerno, I-84084 Fisciano (Sa), Italy
[3]Department of Imaging Physics (ImPhys), Faculty of Applied Sciences, Delft University of Technology, Delft 2628 CJ, The Netherlands
[4]Centro NANO_MATES, Università degli Studi di Salerno, I-84084 Fisciano (Sa), Italy

[a)]**Author to whom correspondence should be addressed:** carla.cirillo@spin.cnr.it

ABSTRACT

The influence of the reactive DC sputtering parameters on the superconducting properties of NbReN ultrathin films was investigated. A detailed study of the current–voltage characteristics of the plasma was performed to optimize the superconducting critical temperature, T_c. The thickness dependence of T_c for the films deposited under different conditions was analyzed down to the ultrathin limit. Optimized films were used to fabricate superconducting nanowire single photon detectors which, at $T = 3.5$ K, show saturated internal detection efficiency (IDE) up to a wavelength of 1301 nm and 95% IDE at 1548 nm with recovery times and timing jitter of about 8 ns and 28 ps, respectively.

Superconducting nanowire single photon detectors (SNSPDs)[1] are one of the key enabling technologies of many quantum-based application, from computation to cryptography.[2] Other strategic operation fields include space to ground communication,[3] monitoring of atmospheric pollution,[4] medical sensing,[5,6] while further unconventional applications are still at their earlier stage.[7] As a consequence, many efforts are put to enhance specific performance of these devices, depending on their operation field.[8] New platforms and configurations, for example superconductor/superconductor bilayers,[9] Josephson junctions-based single photon detectors,[10] even integrated with innovative materials such as graphene,[11] or carbon nanotubes,[12] were proposed. At the same time, material-oriented research makes continuous progress in the development of these devices.[8,13] For example, in order to meet specific application requirements,[14–18] research still focuses on the optimization of crystalline superconductors with high critical temperature, T_c, such as NbN and NbTiN ($T_c \approx 16$ K), despite their excellent performance as SNSPDs at 1550 nm. Therefore, ion bombardment during sputtering deposition was used to obtain NbN films with increased low temperature resistivity (ρ) and reduced T_c for the realization of SNSPDs with 100% detection efficiency typical of devices made of amorphous superconductors, with the excellent timing performance and higher operating temperatures characteristic of polycrystalline detectors.[19] Moreover, alternative superconductors are constantly suggested. Indeed, recent studies have explored crystalline nitrides such as MoN[20] and VN.[21] Similarly, we are currently investigating NbReN, a new nitride superconductor recently synthesized in form of polycrystalline films with grains of small dimensions, typically 2–3 nm, and bulk T_c of about 5 K.[22] Its electrical transport properties, typical of dirty superconductors, may in principle be of interest in the field of superconducting electronics, in particular for the realization of SNSPDs or high kinetic inductance devices.[23] Its parent compound NbRe[24,25] already demonstrated high performances for the realization of single photon detectors both in forms of nanometric meanders[26] and microstrips.[27–29] Compared with NbRe, NbReN films feature higher resistivity values, and reduced superconducting critical temperature,[22] comparable to those of amorphous superconductors.[30–32] These characteristics may reasonably offer the opportunity to operate NbReN-based detectors in the mid-infrared (MIR) spectral range. In the MIR regime, NbReN could be competitive with amorphous superconductors, such as WSi[30,31] or MoSi,[32] which typically suffer from poor time resolution and very low operation temperature. In contrast, NbReN-based detectors are expected to present

excellent time performances, as its parent compound,[22] due to the low values of the quasiparticle relaxation times estimated from flux-flow instability study.[33] Here, we report on the first SNSPD based on NbReN films. First, we illustrate the simple yet reliable deposition process developed to correlate the sputtering conditions to the electrical properties of the films both in the normal and superconducting states. The deposition conditions were tuned to produce ultrathin NbReN films with T_c values suitable to operate the detector at temperatures reachable with commercial cryogen free systems. As a result, nanometric meanders, with wires about 70 nm wide and circular detection area with a radius of about 4 μm based on 10-nm-thick NbReN films, show 95% IDE at 1550 nm and excellent time performance at 3.5 K.

NbReN films were deposited on Si substrates in a UHV DC magnetron sputtering system with a base pressure of about 2×10^{-8} mbar. A stoichiometric NbRe ($Nb_{0.18}Re_{0.82}$) target (99.95% pure, 5 cm in diameter) was reactively sputtered in a mixture of argon (Ar, 99.95% pure, inert gas) and nitrogen (N_2, 99.95% pure, reactive gas), whose relative concentration was finely tuned using two mass flow controllers. The total deposition pressure, p_{tot}, was measured by a capacitive gauge. Finally, sputtering was performed in a power bias mode.

Following Refs. 20, 34, and 35, the analysis of discharge parameters was performed. Indeed, different deposition conditions result in different plasma properties. In particular, the influence of the amount of nitrogen gas and the sputtering power (P), crucial in determining film properties, was carefully examined. For this purpose, more than 100 films of different thickness (d_{NbReN}) were grown. They were schematically divided into three sets based on the growth regime, as reported in Table I. The series named A comprises the films analyzed in Ref. 22. They were deposited in the regime of high N_2 fraction [$N_2^{\%}$=N_2/(N_2+Ar)] and low P. On the contrary, the series named as B (C) was obtained for intermediate (low) $N_2^{\%}$ values and high (low) P. After optimizing the deposition conditions for each set, we deposited films with thicknesses down to the ultrathin limit as required for the realization of SNSPDs. All depositions were performed in the regime corresponding to the formation of nitride compound at the target.[36] During this process, the target voltage (V) changes accordingly. In particular, once both the Ar pressure (p_{Ar}) and P are fixed, V increases as a function of the N_2 fraction[34,37] due to higher impedance of the compound with respect to the metallic target.[38] As reported in Refs. 34 and 37 the maximum value of T_c is observed where a steep increase appears in the $V(N_2^{\%})$ dependence. This effect was initially observed in the films of the A series, as reported in Fig. S1 (see the supplementary material). However, the films of this set have lower T_c compared to the native NbRe. For example, NbReN films 8-nm-thick deposited under optimized conditions have a T_c of about 4 K,[22] whereas NbRe films of the same thickness used to realize the first SNSPDs have $T_c = 6$ K.[26]

TABLE I. Deposition conditions and film thicknesses for the series of samples under investigation.

Series name	P_{tot}(μbar)	$N_2^{\%}$(μbar)	P(W)	d_{NbReN}(nm)
A (Ref. 22)	4.5–13	23–44	100–150	4–70
B	3.0–4.2	9–29	150–350	5–50
C	3.5–6.3	2.8–6.0	40–200	6–50

In order to increase T_c in the ultrathin film regime, for the new series (B and C) we analyzed the discharge characteristics obtained in different sputtering regimes. The dependence of plasma current on the discharge voltage was systematically monitored both as a function of P and nitrogen content. In the case of B series, we fixed $p_{Ar} = 3$ μbar. Figure 1(a) shows the dependence of current (I) on V, as a function of P and with the addition of different N_2 fractions, from a pure Ar atmosphere (black curve, thick line) up to $N_2^{\%} = 29\%$ (magenta curve). The results show that I always increases with V, exhibiting an almost linear relationship for pure NbRe, but showing slight curvature when reactive processes occur. As discussed in Ref. 35 in the case of NbN, the optimal deposition occurs for negative $I - V$ slopes, namely when a dynamic equilibrium between the nitride formation at the target surface and its erosion is established. The first process is controlled by the amount of N_2 and independent of I, the second, on the contrary, is an increasing function of I (or P) and dominates at high currents. In our experiments, the $I(V)$ curves of the reactive process did not tend to converge with the $I(V)$ characteristic of the metallic phase, as reported in Refs. 34 and 35 probably due to the characteristics of our deposition system (target dimensions, pumping speed, and maximum P). Our sputtering conditions are instead more similar to that recently reported for MoN films.[20] It is also worth noting that no hysteresis is observed in the $I - V$ curves, probably due to the small target diameter or the pumping speed set during deposition.[34] The critical temperatures of the NbReN 15-nm-thick films deposited under the conditions described by the $I - V$ curves of Fig. 1(a) are reported in the graph. The T_c values were determined as the midpoint of the resistive transitions, $R(T)$. The $R(T)$ curves normalized to the value of the resistance at $T = 20$ K (R_{20K}) for the films deposited at 350 W at different N_2 fractions are reported in Fig. 1(b). In these conditions, we observe a decrease in T_c with increase in $N_2^{\%}$. The values of ρ for these films varies between 140 and 180 $\mu\Omega$cm. With the nitrogen content fixed at $N_2^{\%} = 25$ the dependence of T_c on P was investigated at 150, 250, and 350 W [see open triangles in Fig. 1(a) and violet curves in Fig. 1(b)]. We notice a larger T_c value for $P = 250$ W [thick violet line in Fig. 1(b)], which lies in the more rounded region of the $I - V$ characteristic. This is in accordance with Ref. 35 and may be indicative of the occurrence of the dynamic equilibrium previously discussed at this P value.

Since we could not observe full deviation from the compound to the metallic branch in the $I - V$ curves in the case of series B, we decided to move to a regime of lower power and nitrogen flow (set C). We started by analyzing the $V(N_2^{\%})$ curves at different P. As an example, in the inset of Fig. 2(a) we plot the dependence of plasma voltage as a function of $N_2^{\%}$ for $p_{Ar} = 3.5$ μbar and $P = 50$ W. A clear jump is obtained at a flow of 0.12 sccm. A similar behavior was observed across a wide range of power (data not reported here). Therefore, we restricted ourselves to this nitrogen fraction and constructed the corresponding $I - V$ characteristic by changing P. This result is shown in the main panel of Fig. 2(a). Here, the $I - V$ curve in pure Ar (squares) is compared to the reactive characteristics (circles). Even if the two branches are now very close, it is possible to observe that they have different shapes. At very low power they exhibit different concavities, while they tend to merge in the high power limit. In the intermediate regime, between about 40 and 80 W (as indicated by the blue isopower curves), the characteristics are more distant and a hint of negative resistance is present. As in the case of B series, this plot shows the values of T_c for the films with $d_{NbReN} = 10$ nm deposited at different

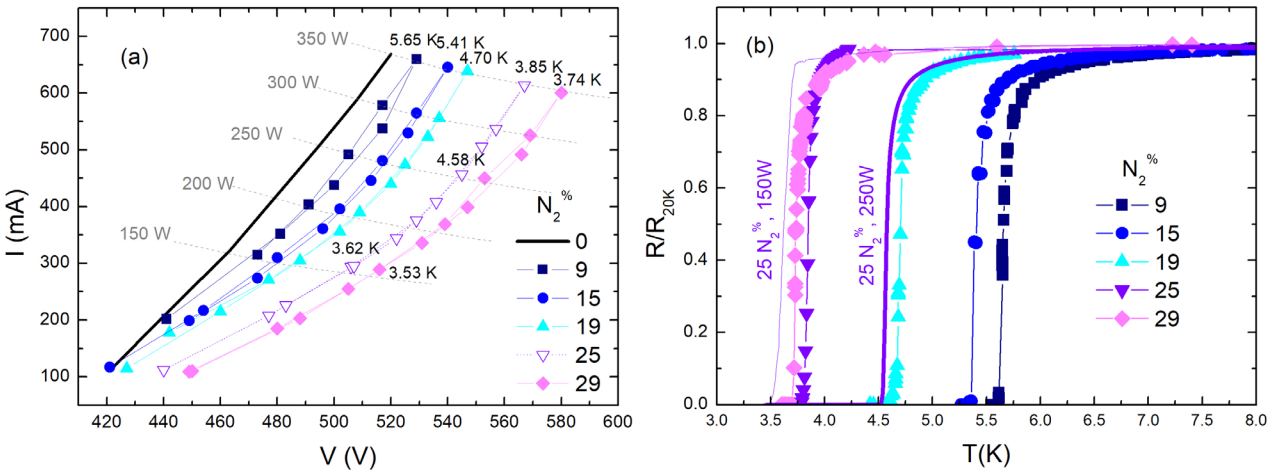

FIG. 1. (a) Current–voltage characteristics for $p_{Ar} = 3$ μbar and different $N_2^{\%}$ by varying the sputtering power, P. The black curve corresponds to the plasma in a pure Ar atmosphere. The dashed lines indicate the isopower curves (see gray labels). Numbers indicate the T_c values of the films 15-nm-thick deposited in the specific conditions. (b) Normalized resistance vs temperature curves for 15-nm-thick films deposited at $p_{Ar} = 3$ μbar, with $P = 350$ W, and varying $N_2^{\%}$ content. Normalized R(T) curves of films deposited with $N_2^{\%} = 25$ both at 150 and 250 W are also shown, represented by thin and thick violet lines, respectively.

powers. In agreement with literature findings,[35] larger values of critical temperature are obtained for films grown in the regime of negative plasma resistance, namely in the region enclosed within the blue curves of Fig. 2(a). Therefore, films of different thicknesses, from $d_{NbReN} = 20$ nm down to the ultrathin limit $d_{NbReN} = 6$ nm, were deposited in these growth conditions. We first analyzed the dependence of ρ on the sputtering power, as reported in Fig. 2(b) for $d_{NbReN} = 6$, 10, and 20 nm. The values of ρ are comparable with those of series B, with a tendency toward increased resistivity for higher power and small d_{NbReN}. Concerning the critical temperature, in Fig. 2(c) the $T_c(P)$ dependence is reported for $d_{NbReN} = 6$, 8, 10, and 20 nm. The curves scale without any crossings, clearly demonstrating a systematic enhancement of the critical temperature with increasing d_{NbReN}. The behaviors are non-monotonous, since the largest T_c is obtained for the film deposited at 50 W for all d_{NbReN}. It is important to stress that by tuning the growth conditions, the values of T_c increased considerably. This is clearly evident from Fig. 3, where we compared the results obtained for the different series of films grown according to the more promising conditions. For example, for $d_{NbReN} = 8$ nm at $P = 50$ W, it is $T_c = 5.25$ K, more than one Kelvin larger than that observed for series A.[22] The $T_c(d_{NbReN})$ dependencies also indicate that growing the films at low $N_2^{\%}$ is particularly beneficial in the ultrathin limit, $d_{NbReN} < 10$ nm, which is relevant for application as SNSPDs.

Superconducting nanowire single-photon detectors were fabricated from a 10-nm-thick NbReN film deposited under regime C at $p_{Ar} = 3.5$ μbar, $N_2^{\%} = 2.8$, and $P = 150$ W. The film shows $T_c = 5.00$ K and resistivity $\rho = 125$ $\mu\Omega$cm. A 100 kV electron beam lithography system (Raith EBPG-5200) was used to define patterns on a 100-nm-thick AR-P 6200 resist. Subsequent structures were etched using reactive ion etching with a gas mixture of SF_6/O_2 (13.5/3.5 sccm flow rates). After fabrication, the remaining resist was removed using wet cleaning (Anisole) and then SNSPDs were covered by a 12 nm

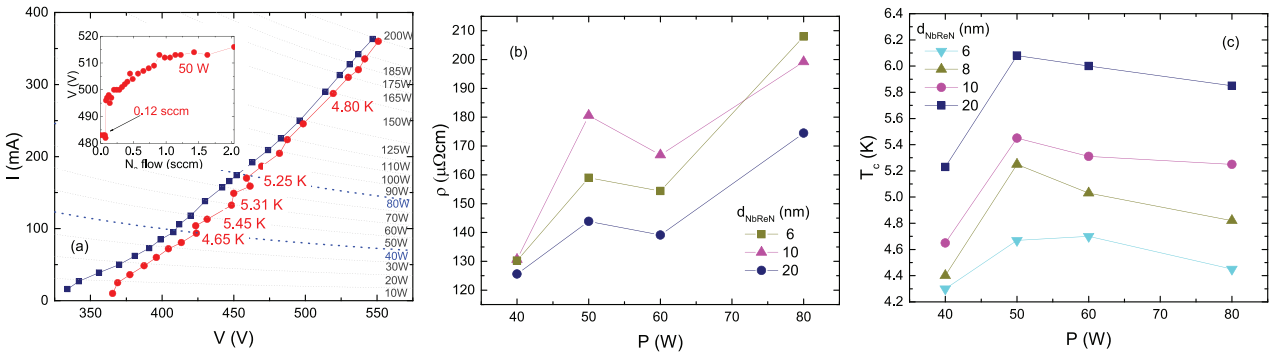

FIG. 2. (a) Current–voltage characteristics for $p_{Ar} = 3.5$ μbar. The navy (red) curve corresponds to the plasma in a pure Ar (for a nitrogen flow of 0.12 sccm, where the jump as a function of the nitrogen flow appears, see inset). The gray lines indicate the isopower curves (see gray labels). The blue isopower lines define the region of negative slope (see the text). Numbers indicate the T_c values of the films deposited in specific conditions for $d_{NbReN} = 10$ nm. (b) Dependence of low temperature resistivity on P for films with thicknesses ranging from 6 to 20 nm, deposited at nitrogen flow rates in the range 0.12–0.24 sccm. (c) Dependence of T_c on the sputtering power for films with thicknesses ranging from 6 to 20 nm deposited under the same conditions as in panel (b).

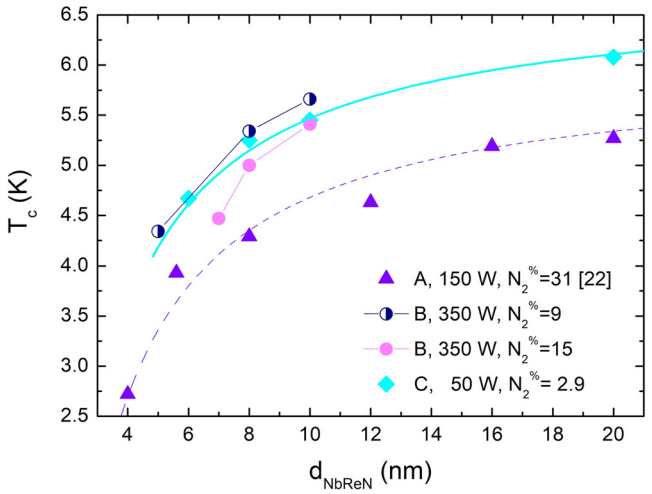

FIG. 3. $T_c(d_{NbReN})$ dependence in the low thickness limit for a selection of films representative of the sample sets under study as indicated in the legend. The lines are guide to the eye.

layer of SiN deposited via plasma-enhanced chemical vapor deposition, to prevent oxidation. The completed devices were mounted in a Gifford–McMahon closed cycle cryostat with base temperature of 3.5 K, and characterized under flood illumination configuration. Among the geometries we tested, the devices with linewidth 70 nm, pitch 140 nm, and radius 4.5 μm showed the best performances, exhibiting IDE saturation at longer wavelengths together with superior timing jitter. For this reason, the corresponding SNSPDs were chosen as representative samples. Scanning Electron Microscope (SEM) image of the selected device is shown in Fig. 4(a). The critical current density of the detector at $T = 3.5$ K is 2.46×10^{10} A/m^2. Photon count rates and dark count rates of the representative SNSPD measured as a function of bias current (I_b) at $T = 3.5$ K ($T/T_c = 0.7$) for wavelengths (λ) from 785 to 1548 nm are presented in Fig. 4(b). The results were normalized with respect to the saturation values of the sigmoid fitting function, and they clearly show saturated IDE for wavelengths up to 1301 nm, and 95% IDE at 1548 nm. This represents a significant improvement with respect to the efficiency of the first NbRe-based SNSPDs. In that case, the best performing device (thickness 8 nm, linewidth 50 nm, pitch 100 nm, and radius 5 μm) at the same wavelength reached a lower saturation of about 89%, despite operating at $T/T_c = 0.5$.[26] In addition to the linear-scale plot, the IDE at 1550 nm is also reported in Fig. 4(c) in logarithmic scale for a visual confirmation of the curve bending as saturation is approached. Characteristic times were measured at $I_b \approx 95\% I_c$ using 1301 nm laser illumination at $T = 3.5$ K via a cryogenic amplification stage and 4 GHz bandwidth oscilloscope. Figure 5(a) shows a single pulse with an exponential decay fit; $t_{rise} = 450$ ps, defined as the time interval between 20% and 80% of the pulse amplitude, and $t_{fall} = 8.00$ ns, from exponential decay fitting. The irregularities observed in the falling edge of the pulse are attributed to reflections within the readout circuitry. It is worth noting that the intrinsic fall time could be shorter than the 8 ns extracted from the exponential fit, as the initial decay appears faster and may be partially masked by reflections. The pulse shape at $T = 2.4$ K measured via a room-temperature amplification stage is reported in the supplementary material as Fig. S3. The timing jitter of another device with the same geometry on the same chip was measured at $T = 3.5$ K, and it is reported in Fig. 5(b). The slightly asymmetric distribution may stem from resistivity variations due to partial oxidation.[44] The measured jitter of this SNSPD is 28.4±0.5 ps at full-width half-maximum (FWHM) of the Gaussian fit. These values are comparable to those of NbRe- and NbTiN-based SNSPDs at $T = 4.3$ K[26,39,45] and outperform some amorphous high-performance materials at similar temperatures.[40–43] Notably, these promising results can be further improved through film tuning and process optimization.[8,39]

In conclusion, NbReN ultrathin films with improved T_c with respect with the first reported samples[22] were deposited by tuning the sputtering conditions. SNSPDs fabricated from these films exhibit 100% IDE up to 1301 nm and 95% IDE at 1548 nm, low timing jitter, and nanosecond recovery times. These results position NbReN as a promising candidate for detectors operating at cryogenic temperatures achievable with compact closed-cycle systems, with potential applicability extending into the MIR. Further optimization of the growth and patterning processes may lead to improved performances, broadening the applicability of this material to quantum technologies.

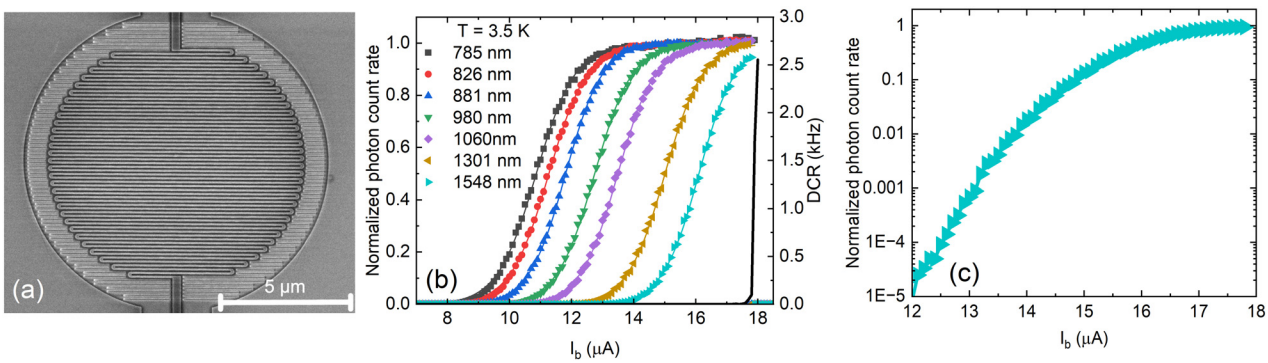

FIG. 4. (a) SEM image of a representative SNSPD device; (b) normalized photon count rate data points (dots) and sigmoidal fittings (lines) for λ ranging from 785 to 1548 nm (left axis) and DCR (right axis) at $T = 3.5$ K; and (c) normalized photon count rate at $\lambda = 1548$ nm and $T = 3.5$ K in logarithmic scale.

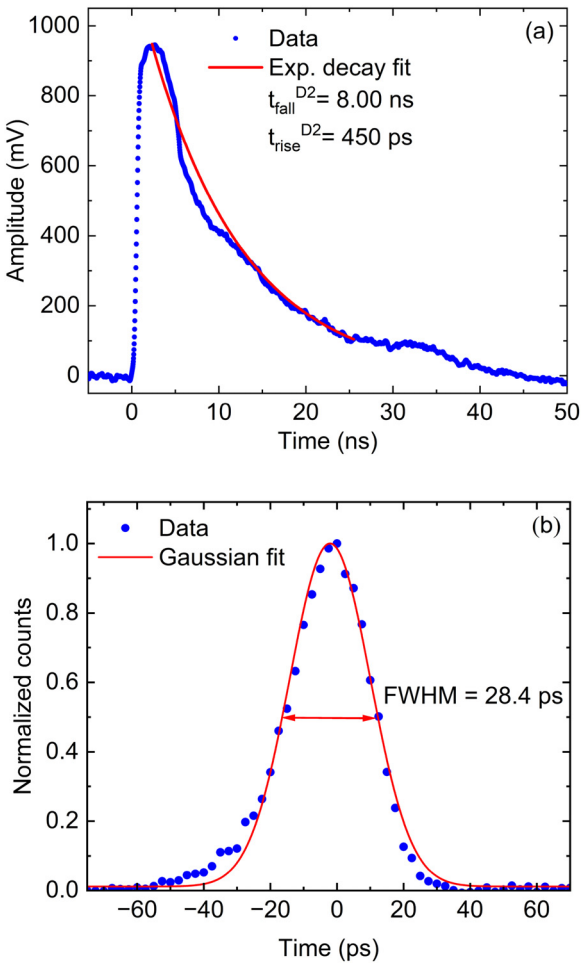

FIG. 5. (a) Single pulse at $T = 3.5$ K (blue), with exponential fit of the decay (red); t_{rise} and t_{fall} are shown. (b) Timing jitter at $T = 3.5$ K for a similar detector; data (points) and Gaussian fit (line).

See the supplementary material for details on the deposition conditions of the A-series films, resistive transitions of films belonging to the C series, and the SNSPD pulse shape recorded at $T = 2.4$ K using a room temperature amplification stage.

This research was partially supported by the QUANCOM Project (MUR PON "Research and Innovation" 2014–2020, No. ARS01_00734) and by the IRIS Project (No. IR0000003), funded by the NextGenerationEU program under the Italian National Recovery and Resilience Plan (Decree of the Ministry of University and Research No. 124, June 21, 2022 – Mission 4, Component 2, Investment 3.1).

AUTHOR DECLARATIONS

Conflict of Interest

The authors have no conflicts to disclose.

Author Contributions

F. Avitabile: Data curation (lead); Investigation (lead); Writing – original draft (equal). **F. Colangelo:** Data curation (lead); Investigation (lead); Writing – original draft (equal). **M. Yu. Mikhailov:** Data curation (equal); Investigation (equal); Writing – review & editing (equal). **Z. Mahdoumi Kakhaki:** Investigation (supporting). **A. Kumar:** Investigation (supporting). **I. Esmaeil Zadeh:** Conceptualization (equal); Supervision (equal); Writing – review & editing (equal). **C. Attanasio:** Conceptualization (equal); Supervision (equal); Writing – review & editing (equal). **C. Cirillo:** Conceptualization (equal); Supervision (equal); Writing – original draft (lead).

DATA AVAILABILITY

The data that support the findings of this study are available from the corresponding author upon reasonable request.

REFERENCES

[1] I. E. Zadeh, J. Chang, J. W. N. Los, S. Gyger, A. W. Elshaari, S. Steinhauer, S. N. Dorenbos, and V. Zwiller, "Superconducting nanowire single-photon detectors: A perspective on evolution, state-of-the-art, future developments, and applications," Appl. Phys. Lett. **118**, 190502 (2021).
[2] L. You, "Superconducting nanowire single-photon detectors for quantum information," Nanophotonics **9**, 2673 (2020).
[3] H. Hao, Q. Y. Zhao, Y. H. Huang, J. Deng, F. Yang, S.-Y. Ru, Z. Liu, C. Wan, H. Liu, Z.-J. Li, H.-B. Wang, X.-C. Tu, J. Chen, L. Kang, and P.-H. Wu, "A compact multi-pixel superconducting nanowire single-photon detector array supporting gigabit space-to-ground communications," Light **13**, 25 (2024).
[4] D. Salvoni, L. Parlato, M. Ejrnaes, F. Mattioli, A. Gaggero, F. Martini, A. Boselli, A. Sannino, S. Amoruso, R. Cristiano, and G. P. Pepe, "Large area SNSPD for lidar measurements in the infrared," IEEE Trans. Appl. Supercond. **32**, 2200304 (2022).
[5] N. Ozana, A. I. Zavriyev, D. Mazumder, M. Robinson, K. Kaya, M. Blackwell, S. A. Carp, and M. A. Franceschini, "Superconducting nanowire single-photon sensing of cerebral blood flow," Neurophotonics **8**, 035006 (2021).
[6] A. Tamimi, M. Caldarola, S. Hambura, J. C. Boffi, N. Noordzij, J. W. N. Los, A. Guardiani, H. Kooiman, L. Wang, C. Kieser, F. Braun, M. A. Usuga Castaneda, A. Fognini, and R. Prevedel, "Deep mouse brain two-photon near-infrared fluorescence imaging using a superconducting nanowire single-photon detector array," ACS Photonics **11**, 3960 (2024).
[7] T. Polakovic, W. Armstrong, G. Karapetrov, Z.-E. Meziani, and V. Novosad, "Unconventional applications of superconducting nanowire single photon detectors," Nanomaterials **10**, 1198 (2020).
[8] I. Holzman and Y. Yachin, "Superconducting nanowires for single-photon detection: Progress, challenges, and opportunities," Adv. Quantum Technol. **2**, 1800058 (2019).
[9] Y. Ivry, J. J. Surick, M. Barzilay, C.-S. Kim, F. Najafi, E. Kalfon-Cohen, A. D. Dane, and K. K. Berggren, "Superconductor-superconductor bilayers for enhancing single-photon detection," Nanotechnology **28**, 435205 (2017).
[10] E. D. Walsh, W. Jung, G.-H. Lee, D. K. Efetov, B.-I. Wu, K.-F. Huang, T. A. Ohki, T. Taniguchi, K. Watanabe, P. Kim, D. Englund, and K. C. Fong, "Josephson junction infrared single-photon detector," Science **372**, 409 (2021).
[11] E. D. Walsh, D. K. Efetov, G.-H. Lee, M. Heuck, J. Crossno, T. A. Ohki, P. Kim, D. Englund, and K. C. Fong, "Graphene-based Josephson-junction single-photon detector," Phys. Rev. Appl. **8**, 024022 (2017).
[12] D. S. Rampini, C. S. Yung, B. G. Oripov, S. Woods, J. Lehman, S. W. Nam, and A. N. McCaughan, "Integration of vertically-aligned carbon nanotubes with superconducting nanowire single photon detectors," Supercond. Sci. Technol. **37**, 015005 (2024).
[13] A. E. Verma and V. B. Horansky *et al.*, "Materials development for high efficiency superconducting nanowire single-photon detectors," MRS Online Proc. Library **1807**, 1 (2015).

[14]R. Cheng, J. Wright, H. G. Xing, D. Jena, and H. X. Tang, "Epitaxial niobium nitride superconducting nanowire single-photon detectors," Appl. Phys. Lett. **117**, 132601 (2020).
[15]I. A. Stepanov, A. S. Baburin, D. V. Kushnev, E. V. Sergeev, O. I. Shmonina, A. R. Matanin, V. V. Echeistov, I. A. Ryzhikov, Y. V. Panfilov, and I. A. Rodionov, "Sputtered NbN films for ultrahigh performance superconducting nanowire single-photon detectors," Appl. Phys. Lett. **12**, 021127 (2024).
[16]J. Zichi, J. Chang, S. Steinhauer, K. von Fieandt, J. W. N. Los, G. Visser, N. Kalhor, T. Lettner, A. W. Elshaari, I. Esmaeil Zadeh, and V. Zwiller, "Optimizing the stoichiometry of ultrathin NbTiN films for high-performance superconducting nanowire single-photon detectors," Opt. Express **27**, 26579 (2019).
[17]W. Shan and S. Ezaki, "Modeling current-voltage characteristics of DC reactive magnetron discharges and its application to superconducting NbTiN film deposition," J. Appl. Phys. **130**, 083302 (2021).
[18]J. Chang, J. Los, R. Gourgues, S. Steinhauer, S. Dorenbos, S. Pereira, H. Urbach, V. Zwiller, and I. E. Zadeh, "Efficient mid-infrared single-photon detection using superconducting NbTiN nanowires with high time resolution in a Gifford-McMahon cryocooler," Photonics Res. **10**, 1063 (2022).
[19]A. E. Dane, A. N. McCaughan, D. Zhu, Q. Zhao, C.-S. Kim, N. Calandri, A. Agarwal, F. Bellei, and K. K. Berggren, "Bias sputtered NbN and superconducting nanowire devices," Appl. Phys. Lett. **111**, 122601 (2017).
[20]L. Hallett, I. Charaev, A. Agarwal, A. Dane, M. Colangelo, D. Zhu, and K. K. Berggren, "Superconducting MoN thin films prepared by DC reactive magnetron sputtering for nanowire single-photon detectors," Supercond. Sci. Technol. **34**, 035012 (2021).
[21]P. Zolotov, A. Semenov, A. Divochiy, and G. Goltsman, "A comparison of VN and NbN thin films towards optimal SNSPD efficiency," IEEE Trans. Appl. Supercond. **31**, 1100804 (2021).
[22]C. Cirillo, V. Granata, A. Spuri, A. Di Bernardo, and C. Attanasio, "NbReN: A disordered superconductor in thin film form for potential application as superconducting nanowire single photon detector," Phys. Rev. Mater. **5**, 085004 (2021).
[23]A. V. Moshe, E. Farber, and G. Deutscher, "Granular superconductors for high kinetic inductance and low loss quantum devices," Appl. Phys. Lett. **117**, 062601 (2020).
[24]C. Cirillo, G. Carapella, M. Salvato, R. Arpaia, M. Caputo, and C. Attanasio, "Superconducting properties of noncentrosymmetric $Nb_{0.18}Re_{0.82}$ thin films probed by transport and tunneling experiments," Phys. Rev. B **94**, 104512 (2016).
[25]M. Caputo, C. Cirillo, and C. Attanasio, "NbRe as candidate material for fast single photon detection," Appl. Phys. Lett. **111**, 192601 (2017).
[26]C. Cirillo, J. Chang, M. Caputo, J. W. N. Los, S. Dorenbos, I. Esmaeil Zadeh, and C. Attanasio, "Superconducting nanowire single photon detectors based on disordered NbRe films," Appl. Phys. Lett. **117**, 172602 (2020).
[27]M. Ejrnaes, C. Cirillo, D. Salvoni, F. Chianese, C. Bruscino, P. Ercolano, A. Cassinese, C. Attanasio, G. P. Pepe, and L. Parlato, "Single photon detection in NbRe superconducting microstrips," Appl. Phys. Lett. **121**, 262601 (2022).
[28]P. Ercolano, C. Cirillo, M. Ejrnaes, F. Chianese, D. Salvoni, C. Bruscino, R. Satariano, A. Cassinese, C. Attanasio, G. P. Pepe, and L. Parlato, "Investigation of dark count rate in NbRe microstrips for single photon detection," Supercond. Sci. Technol. **36**, 105011 (2023).
[29]C. Cirillo, M. Ejrnaes, P. Ercolano, C. Bruscino, A. Cassinese, D. Salvoni, C. Attanasio, G. P. Pepe, and L. Parlato, "Single photon detection up to 2 μm in pair of parallel microstrips based on NbRe ultrathin films," Sci. Rep. **14**, 20345 (2024).
[30]V. B. Verma, B. Korzh, A. B. Walter, A. E. Lita, R. M. Briggs, M. Colangelo, Y. Zhai, E. E. Wollman, A. D. Beyer, J. P. Allmaras, H. Vora, D. Zhu, E. Schmidt, A. G. Kozorezov, K. K. Berggren, R. P. Mirin, S. W. Nam, and M. D. Shaw, "Single-photon detection in the mid-infrared up to 10 μm wavelength using tungsten silicide superconducting nanowire detectors," APL Photonics **6**, 056101 (2021).
[31]M. Colangelo, A. B. Walter, B. A. Korzh, E. Schmidt, B. Bumble, A. E. Lita, A. D. Beyer, J. P. Allmaras, R. M. Briggs, A. G. Kozorezov, E. E. Wollman, M. D. Shaw, and K. K. Berggren, "Large-area superconducting nanowire single-photon detectors for operation at wavelengths up to 7.4 μm," Nano Lett. **22**, 5667 (2022).
[32]Q. Chen, R. Ge, L. Zhang, F. Li, B. Zhang, F. Jin, H. Han, Y. Dai, G. He, Y. Fei, X. Wang, H. Wang, X. Jia, Q. Zhao, X. Tu, L. Kang, J. Chen, and P. Wu, "Mid-infrared single photon detector with superconductor $Mo_{0.8}Si_{0.2}$ nanowire," Sci. Bull. **66**, 965 (2021).
[33]Z. Makhdoumi Kakhaki, A. Leo, A. Spuri, M. Ejrnaes, L. Parlato, G. P. Pepe, F. Avitabile, A. Di Bernardo, A. Nigro, C. Attanasio, and C. Cirillo, "Characterization of quasiparticle relaxation times in microstrips of NbReN for perspective applications for superconducting single-photon detectors," Mater. Sci. Eng., B **304**, 117376 (2024).
[34]B. G. C. Bos, D. J. Thoen, E. A. F. Haalebos, P. M. L. Gimbel, T. M. Klapwijk, J. J. A. Baselmans, and A. Endo, "Reactive magnetron sputter deposition of superconducting Niobium Nitride thin films with different target sizes," IEEE Trans. Appl. Supercond. **27**, 1500405 (2017).
[35]D. Henrich, S. Dorner, M. Hofherr, K. Il'in, A. Semenov, E. Heintze, M. Scheffler, M. Dressel, and M. Siegel, "Broadening of hot-spot response spectrum of superconducting NbN nanowire single-photon detector with reduced nitrogen content," J. Appl. Phys. **112**, 074511 (2012).
[36]M. Ohring, *Materials Science of Thin Films* (Elsevier, 1992).
[37]D. M. Glowacka, D. J. Goldie, S. Withington, H. Muhammad, G. Yassin, and B. K. Tan, Development of a NbN deposition process for superconducting quantum sensors, arXiv:1401.2292v1 (2014).
[38]T. Matsunaga, H. Maezawa, and T. Noguchi, "Characterization of NbTiN thin films prepared by reactive DC-magnetron sputtering," IEEE Trans. Appl. Supercond. **13**, 3284 (2003).
[39]I. E. Zadeh, J. W. N. Los, R. B. M. Gourgues, V. Steinmetz, G. Bulgarini, S. M. Dobrovolskiy, V. Zwiller, and S. N. Dorenbos, "Single-photon detectors combining high efficiency, high detection rates, and ultra-high timing resolution," APL Photonics **2**, 111301 (2017).
[40]F. Marsili, V. B. Verma, J. A. Stern, S. Harrington, A. E. Lita, T. Gerrits, I. Vayshenker, B. Baek, M. D. Shaw, R. P. Mirin, and S. W. Nam, "Detecting single infrared photons with 93% system efficiency," Nat. Photonics **7**, 210–214 (2013).
[41]V. B. Verma, A. E. Lita, M. R. Vissers, F. Marsili, D. P. Pappas, R. P. Mirin, and S. W. Nam, "Superconducting nanowire single photon detectors fabricated from an amorphous $Mo_{0.75}Ge_{0.25}$ thin film," Appl. Phys. Lett. **105**, 022602 (2014).
[42]Yu. P. Korneeva, M. Yu. Mikhailov, Yu. P. Pershin, N. N. Manova, A. V. Divochiy, Yu. B. Vakhtomin, A. A. Korneev, K. V. Smirnov, A. G. Sivakov, A. Y. Devizenko, and G. N. Goltsman, "Superconducting single-photon detector made of MoSi film," Supercond. Sci. Technol. **27**, 095012 (2014).
[43]J. Chiles, S. M. Buckley, A. Lita, V. B. Verma, J. Allmaras, B. Korzh, M. D. Shaw, J. M. Shainline, R. P. Mirin, and S. W. Nam, "Superconducting microwire detectors based on WSi with single-photon sensitivity in the near-infrared," Appl. Phys. Lett. **116**, 242602 (2020).
[44]I. E. Zadeh, J. W. N. Los, R. B. M. Gourgues, J. Chang, A. W. Elshaari, J. R. Zichi, Y. J. van Staaden, J. P. E. Swens, N. Kalhor, A. Guardiani, Y. Meng, K. Zou, S. Dobrovolskiy, A. W. Fognini, D. R. Schaart, D. Dalacu, P. J. Poole, M. E. Reimer, X. Hu, S. F. Pereira, V. Zwiller, and S. N. Dorenbos, "Efficient single-photon detection with 7.7 ps time resolution for photon-correlation measurements," ACS Photonics **7**, 1780 (2020).
[45]R. B. M. Gourgues, J. W. N. Los, J. Zichi, J. Chang, N. Kalhor, G. Bulgarini, S. N. Dorenbos, V. Zwiller, and I. E. Zadeh, "Superconducting nanowire single photon detectors operating at temperature from 4 to 7 K," Opt. Express **27**, 24601 (2019).